



HAL
open science

Time-delayed interactions on acoustically driven bubbly screens

Yuzhen Fan, Haisen Li, Daniel Fuster

► **To cite this version:**

Yuzhen Fan, Haisen Li, Daniel Fuster. Time-delayed interactions on acoustically driven bubbly screens. Journal of the Acoustical Society of America, 2021. hal-03834534

HAL Id: hal-03834534

<https://hal.science/hal-03834534>

Submitted on 30 Oct 2022

HAL is a multi-disciplinary open access archive for the deposit and dissemination of scientific research documents, whether they are published or not. The documents may come from teaching and research institutions in France or abroad, or from public or private research centers.

L'archive ouverte pluridisciplinaire **HAL**, est destinée au dépôt et à la diffusion de documents scientifiques de niveau recherche, publiés ou non, émanant des établissements d'enseignement et de recherche français ou étrangers, des laboratoires publics ou privés.

Time-delayed interactions on acoustically driven bubbly screens

Yuzhe Fan,^{1, a)} Haisen Li,^{1, b)} and Daniel Fuster^{2, c)}

¹⁾*Acoustic Science and Technology Laboratory, Harbin Engineering University,
Harbin 150001, China*

²⁾*Sorbonne Universités, UPMC Univ Paris 06, CNRS,
UMR 7190, Institut Jean Le Rond d'Alembert, F-75005 Paris,
France*

(Dated: 5 November 2021)

1 We discuss the influence of compressibility effects including time delays on the dy-
2 namics of acoustically excited bubbly screens. In the linear regime we show that
3 the proposed model for the infinite bubbly screen recovers the results predicted by
4 the effective medium theory up to the second order without introducing any fit-
5 ting parameter when the wavelength is large compared to the inter-bubble distance.
6 However, the effect of boundaries on finite bubbly screens is shown to lead to the
7 appearance of multiple local resonances and characteristic periodic structures that
8 limit the applicability of the effective medium theory. In addition a local resonance
9 phenomenon in the liquid spacings between bubbles is observed for both infinite and
10 finite bubbly screens with crystal structures, these effects vanishing as the crystal
11 structure is perturbed. In the non-linear regime, we treat the current model with
12 time-delay effects as a delay differential equation that is directly solved numerically.
13 We show the appearance of **an** optimal distance for subharmonic emission for crystal
14 structures and discuss the accuracy of effective medium theory in the strong non-
15 linear regime.

a) Also at: College of Underwater Acoustic Engineering, Harbin Engineering University, Harbin 150001, China

b) Also at: Key Laboratory of Marine Information Acquisition and Security (Harbin Engineering University),
Ministry of Industry and Information Technology, Harbin 150001, China

c) fuster@dalembert.upmc.fr

16 I. INTRODUCTION

17 The dynamics of cavities in liquids has attracted a lot of interest over the past few decades
18 (Fuster, 2019; Lohse, 2018). The oscillation of an isolated bubble is well described by the
19 Rayleigh-Plesset (RP) like equation that accounts for compressibility effects (Gilmore, 1952;
20 Keller and Miksis, 1980; Lauterborn and Kurz, 2010; Prosperetti *et al.*, 1986). However,
21 bubbles often appear in ensembles, and bubble-bubble interactions need to be accounted as
22 the bubble interface acceleration influences the pressure distribution in the bubble surround-
23 ings. One traditional way to account for the influence of interactions is to use the effective
24 medium method. Foldy (1945), Caffisch *et al.* (1985), and Commander and Prosperetti
25 (1989) consider the influence that the dynamic bubble response have on the effective prop-
26 erties of a wave propagating in a bubbly liquid. The multiple interactions among bubbles are
27 described by the interaction between each bubble and the averaged pressure field. However
28 these models are limited to diluted systems and frequencies for which the wavelength is
29 larger than the characteristic bubble radius and the inter-bubble distance.

30

31 In an attempt to generalize the range of applicability of these theories to shorter wave-
32 lengths and capture more accurately the interaction mechanisms among bubbles, some
33 authors propose to solve a coupled system of RP like equations (Fan *et al.*, 2020b; Fuster
34 and Colonius, 2011; Ilinskii *et al.*, 2007; Mettin *et al.*, 1997). These approaches can be even-
35 tually coupled with an Eulerian-Lagrangian approach (Fuster and Colonius, 2011; Maeda
36 and Colonius, 2019) to capture both short and long wave range interactions and can be

37 considered as two-way coupled model, where bubbles can directly feel the acoustic field
38 emitted by each other. An intrinsic difficulty in these models is how to account for the
39 influence of the liquid compressibility on the multiple interactions among bubbles. Indeed
40 one of the most frequently-used assumption is to resort to the incompressible limit, where
41 we neglects any time-delay effect due to liquid compressibility and the interactions among
42 bubbles take place instantaneously . Although this assumption is certainly valid when the
43 wavelength of the excitation pressure wave is much larger than the characteristic size of the
44 bubble cluster, the accuracy of applicability of these models in systems with many bubbles
45 has not been discussed in detail.

46
47 Some numerical studies applied to medical related research such as high-intensity fo-
48 cused ultrasound (Okita *et al.*, 2013), ultrasound contrast agent (Faez *et al.*, 2012), and
49 drug delivery (Coussios and Roy, 2008) point out the importance of compressibility effects,
50 in particular time-delay effects in real applications (Sujarittam and Choi, 2020). More
51 fundamental studies including experimental works studying the acoustic propagation in the
52 vicinity of a bubble chain (Manasseh *et al.*, 2004) have shown that the time-delay effects
53 considerably change the resonance frequencies and the damping factors of the effective
54 medium (Doinikov *et al.*, 2005; Ooi *et al.*, 2008), so does bubble near boundaries (Dahl and
55 Kapodistrias, 2003; van't Wout and Feuillade, 2021; Ye and Feuillade, 1997). In the context
56 of the development of acoustic metamaterials, two-dimensional bubble layers also known
57 as bubbly screens have also become a widely investigated system since 2009 in a series of
58 papers published by Leroy and coworkers (Leroy *et al.*, 2015, 2009; Lombard *et al.*, 2015).

59 Using the self-consistent approach based on the effective medium theory, the transmission
60 and reflection coefficient measured experimentally in the linear regime can be well captured
61 by accounting for the influence of time-delay effects on the interaction term among bubbles.
62 In the non-linear regime, the asymptotic analysis based on effective medium theory (Miksis
63 and Ting, 1989; Pham *et al.*, 2021) have shed light into the role of compressibility on the
64 mechanisms of multiple interactions among bubbles. However, these models still face some
65 challenges. For example, it is known that, even in the dilute limit, crystal configuration
66 has special acoustic properties (Devaud *et al.*, 2010), but the capability of effective medium
67 theory to distinguish between the properties of specific configurations (e.g. crystals) and
68 the ensemble average of randomly distributed systems has not been clarified . Also, it is
69 not clear how well averaged models capture the influence of boundary effects as well as
70 polydispersity effects.

71

72 In this work we discuss the applicability and the accuracy of models based on a coupled
73 system of RP like equations to capture the response of bubbly screens (Figure 1). Section
74 II presents a particularization of the system of Rayleigh-Plesset like equations proposed in
75 Fuster and Colonius (2011) to solve for the dynamic response of the bubbles. In Section III
76 , we show that, without the need of introducing any fitting parameter, this model is able
77 to recover the second order solution predicted by the effective medium theory in the linear
78 oscillating regime for a monodisperse bubbly screen in crystal configuration when the acous-
79 tic excitation wavelength is much larger than both the bubble radius and the inter-bubble
80 distance. Then, we discuss the influence of boundary effects and randomness on the accu-

81 racy of the predictions in comparison with the effective medium theory in the linear regime.
 82 **Finally, in Section IV,** we present numerical results obtained in the non-linear regime using
 83 a delay differential equation solver. These examples reveal the importance of compressibility
 84 effects to correctly predict the non-linear bubble dynamic response.

85 II. BUBBLY SCREEN MODEL

86 The dynamics of an oscillating spherical bubble is described using the Keller-Miksis like
 87 equation (Keller and Miksis, 1980) which is a differential equation for the bubble radius of
 88 the i th bubble in a weakly compressible liquid characterized by its speed of sound c and
 89 density ρ

$$\rho \left(R_i \ddot{R}_i \left(1 - \frac{\dot{R}_i}{c} \right) + \frac{3\dot{R}_i^2}{2} \left(1 - \frac{\dot{R}_i}{3c} \right) \right) - \left(1 + \frac{\dot{R}_i}{c} + \frac{R_i}{c} \frac{d}{dt} \right) (p_{i,B} - p_\infty) = \rho I_i. \quad (1)$$

90 In the equation above, $p_\infty(t) = p_0 + f(t)$ is the pressure excitation; $p_{i,B}$ is the liquid pressure
 91 at the interface of the i th bubble, which we describe using a simple polytropic law $p_{i,B} =$
 92 $\left(p_0 + \frac{2\sigma}{R_{i,0}} \right) \left(\frac{R_{i,0}}{R_i} \right)^{3\kappa} - \frac{2\sigma}{R_i} - \frac{4\mu\dot{R}_i}{R_i}$, where κ is the polytropic index; p_0 is the static pressure;
 93 $R_{i,0}$ is the i th bubble radius at equilibrium; σ is the surface tension; μ is the liquid viscosity.
 94 The interaction term ρI_i represents the pressure fluctuation induced by the presence of the
 95 surrounding bubbles, which has to be evaluated at the deferred time $t_{d_{ij}} = t - d_{ij}/c$, where
 96 $d_{ij} = |\vec{x}_i - \vec{x}_j|$ represents the distance from the i th bubble located at \vec{x}_i to the j th bubble
 97 located at \vec{x}_j . Following Fuster and Colonius (2011), it can be readily shown that

$$I_i = I_{i,0} + I_{i,1}, \quad (2)$$

98 where both terms have to be evaluated at the deferred time $t_{d_{ij}}$

$$\begin{aligned}
I_{i,0} &= - \sum_{j \neq i}^N \frac{R_j(t_{d_{ij}})}{d_{ij}} \left(R_j(t_{d_{ij}}) \ddot{R}_j(t_{d_{ij}}) + 2\dot{R}_j(t_{d_{ij}})^2 \right), \\
I_{i,1} &= - \frac{1}{c} \left[\sum_{j \neq i}^N \frac{R_j(t_{d_{ij}})}{d_{ij}} \dot{R}_j(t_{d_{ij}}) \left[R_j(t_{d_{ij}}) \ddot{R}_j(t_{d_{ij}}) + \frac{\dot{R}_j(t_{d_{ij}})^2}{2} - \frac{(p_{j,B}(t_{d_{ij}}) - p_\infty(t_{d_{ij}}))}{\rho} \right] \right. \\
&\quad \left. - \sum_{j \neq i}^N \frac{R_j(t_{d_{ij}})^2}{d_{ij}} \frac{d}{dt} \frac{(p_{j,B}(t_{d_{ij}}) - p_\infty(t_{d_{ij}}))}{\rho} + \dot{R}_i(t_{d_{ij}}) I_{i,0} \right]. \tag{3}
\end{aligned}$$

99 In the equations above, we only keep first order compressibility correction terms in the
100 intensity of the collapse of bubbles, which scale as a function of the Mach number $Ma = \frac{\dot{R}}{c}$,
101 and time-delay effects. Neglecting time-delay effects (e.g. $t_{d_{ij}} = t$) leads to a coupled system
102 of ordinary differential equations that need to be solved. In the limit of $c \rightarrow \infty$, we recover
103 the classical form of the interaction term $I_i \approx I_{i,0}$ evaluated at t (Bremond *et al.*, 2006; Ida
104 *et al.*, 2007; Yasui *et al.*, 2008). Otherwise, as explained in Section IV, it is required to solve
105 a differential equation with time delays.

106

107 **For monodisperse bubbles, where $R_{i,0} = R_{j,0} = R_0$, the development of liquid compress-**
108 **ibility corrections is typically discussed in terms of the nondimensional wavenumber kR_0 ,**
109 **where $k = \omega/c$. For air/water systems at constant reference pressure, $kR_0 = \frac{\omega}{\omega_0} \frac{1}{c} \sqrt{\frac{3\kappa p_0}{\rho}}$**
110 **depends on the frequency ratio between the excitation frequency, ω , and the resonance**
111 **frequency of single isolated oscillating bubble, $\omega_0 = \sqrt{\frac{3\kappa p_0}{R_0^2 \rho}}$. For air bubbles in water at**
112 **atmospheric conditions, $\frac{1}{c} \sqrt{\frac{3\kappa p_0}{\rho}} \approx 10^{-2}$ (this parameter will be held constant in the follow-**
113 **ing solution for particular configurations of the bubbly screen), and, therefore, kR_0 is small**
114 **except for very high frequencies. However, in addition to kR_0 , it is useful to introduce an al-**
115 **ternative dimensionless wavenumber using the inter-bubble distance D ($kD = \frac{D}{R_0} \frac{\omega}{\omega_0} \frac{1}{c} \sqrt{\frac{3\kappa p_0}{\rho}}$)**

116 which is not always small in diluted systems. kD , kR_0 and $\frac{D}{R_0}$ construct the ratio of the
 117 three relevant spatial scales (the wavelength, the inter-bubble distance, and the bubble
 118 equilibrium radius) considered in this work to characterize the bubble screen.

119

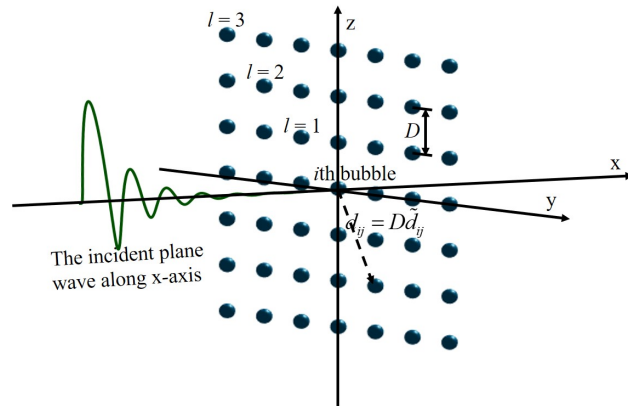


FIG. 1. A typical crystal distributed bubbly screen located at $x = 0$ plane.

120 The particular arrangement of bubbles considered in this work is that of a finite/infinite
 121 bubbly screen (Figure 1) in which bubbles are located in the $x = 0$ plane, perpendicular
 122 to the incident wave, in layers around a central bubble. Any bubble under consideration
 123 will always be labelled with subscript i . In the l th layer, bubbles are equally spaced with
 124 a given inter-bubble distance D along a square of size $2lD$ centered at the bubble under
 125 consideration. The position and the dispersity of the bubbles will be eventually perturbed
 126 when discussing randomization effects in the linear regime.

127 III. COMPRESSIBILITY EFFECTS IN THE LINEAR OSCILLATION REGIME

128 A. General case

129 We start considering the dynamics of a finite bubbly screen with monodisperse bubbles
 130 excited by a weak perturbation, where $R_{i,0} = R_{j,0} = R_0$. For a system with N bubbles,
 131 Eq. 1 reduces to

$$R_i \ddot{R}_i - \left(1 + \frac{R_i}{c} \frac{d}{dt}\right) \frac{p_{i,B} - p_\infty}{\rho} = - \sum_{j \neq i}^N \frac{R_j^2(t_{d_{ij}})}{d_{ij}} \ddot{R}_j(t_{d_{ij}}) + \sum_{j \neq i}^N \frac{R_j(t_{d_{ij}})}{d_{ij}} \frac{R_j(t_{d_{ij}})}{c} \frac{d}{dt} \frac{(p_{j,B}(t_{d_{ij}}) - p_\infty(t_{d_{ij}}))}{\rho}. \quad (4)$$

132 Note that in the linear regime, the influence of the compressibility correction term in the
 133 interaction is not null, and it is not sufficient to retain the classical interaction term $I_{i,0}$ only.

134 For a general case where the pressure at the location of the i th bubble is presented as
 135 $p_\infty(\mathbf{x}_i, t) = p_0(1 + p'_i e^{i\omega t})$, the solution of the equation for the i th bubble can be expressed
 136 in the form of $R_i(t) = R_0(1 + r'_i e^{i\omega t})$. Taking $R_j(t_{d_{ij}}) = R_0(1 + r'_j e^{i\omega(t-d_{ij}/c)})$, the values of r'_i
 137 are obtained from the solution of a linear system, which in indicial notation can be written
 138 as

$$\left(A_{ij}^{(0)} + i k R_0 A_{ij}^{(1)}\right) r'_j = - \frac{p_0}{\rho R_0^2 \omega_0^2} p'_i. \quad (5)$$

139 The coefficients of the matrices $\mathbf{A}^{(0)}$ and $\mathbf{A}^{(1)}$ are given in Appendix A neglecting viscous,
 140 thermal, mass transfer and surface tension terms as well as terms of order $(kR_0)^2$ during
 141 linear analysis. The first choice is justified by the fact that the influence of interactions on
 142 the bubble dynamics can be discussed as a correction of the resonance frequency and the
 143 radiative damping introduced by compressibility effects (Leroy *et al.*, 2009; Pham *et al.*,
 144 2021). For a particular application, it would be straightforward to extrapolate the results

145 to situations where the influence of the effects neglected are relevant using corrected lin-
 146 ear expressions to express the bubble pressure (Bergamasco , 2017; Fuster and Montel,
 147 2015). Neglecting $(kR_0)^2$ terms is justified by the fact that $kR_0 \approx 10^{-2} \frac{\omega}{\omega_0}$ is usually small,
 148 and ignoring higher order terms is a valid assumption except for extremely high frequen-
 149 cies. In this simplified case, matrices $\mathbf{A}^{(0)}$ and $\mathbf{A}^{(1)}$ only depend on the local variable
 150 $\mathfrak{K}_i = \frac{R_0}{D} \sum_{j \neq i}^N \frac{e^{-ikD\tilde{d}_{ij}}}{\tilde{d}_{ij}}$, which represents the strength of the interaction term and depend on
 151 the nondimensional distance $\tilde{d}_{ij} = |\vec{x}_i - \vec{x}_j|/D$.

152

153 For a planar wave, the linear set of equations in Eq. 5 can be numerically solved for an
 154 arbitrary constant value of $p'_i = p'_j = p'$ for all bubbles to find all r'_i . Once these values are
 155 obtained, we can re-express any equation in the system as

$$(-\omega^2 - K_i^* \omega^2 + \omega_0^2) r'_i = -\frac{p_0}{\rho R_0^2} p', \quad (6)$$

156 where, for any arbitrary i th bubble under consideration, we have

$$K_i^* = \mathfrak{K}_i(1 - Q_i^*) - ikR_0 \left[(1 + \mathfrak{K}_i)^2 - \mathfrak{K}_i Q_i^* \left(1 + \mathfrak{K}_i + \frac{\omega_0^2}{\omega^2} \right) \right], \quad (7a)$$

$$Q_i^* = \frac{\sum_{j \neq i}^N (r'_i - r'_j) \frac{e^{-ikD\tilde{d}_{ij}}}{\tilde{d}_{ij}}}{r'_i \sum_{j \neq i}^N \frac{e^{-ikD\tilde{d}_{ij}}}{\tilde{d}_{ij}}}. \quad (7b)$$

157 Equation 6 is similar to the harmonic form of single bubble situation

$$(-\omega^2 + i\zeta_i \omega^2 + \omega_{i,res}^2) r'_i = -\frac{p_0}{\rho R_0^2} p', \quad (8)$$

158 where the local bubble resonance frequency and the local damping factors can be readily
 159 obtained as

$$\omega_{i,res}^2 = \omega_0^2 \left(1 - \Re(K_i^*) \left(\frac{\omega}{\omega_0} \right)^2 \right); \quad \zeta_i = -\Im(K_i^*). \quad (9)$$

160 Function K_i^* gathers both interaction and compressibility effects in the bubble resonance
 161 and the damping of the bubble and depends on the quantity Q_i^* which provides a measure
 162 of the correlation between the radial bubble motion of the i th bubble and that of the sur-
 163 rounding bubbles. Q_i^* becomes zero in the limiting case of synchronous motion. It is also
 164 easy to verify that in the limit of an isolated bubble, $\mathfrak{K}_i \rightarrow 0$, we recover the well known
 165 result, $\omega_{i,res}^2 = \omega_0^2$ and $\zeta_i = \zeta = kR_0$, representing the harmonic oscillation of a single bubble
 166 in a slightly compressible liquid. For systems where K_i^* is not uniform for all the bubbles,
 167 multiple local resonances appear.

168

169 To characterize the global response of the screen, it is useful to express the averaged gas
 170 volume evolution as a function of the amplitude of the driving pressure

$$(-\omega^2 + i\zeta\omega^2 + \omega_{res}^2) \frac{1}{N} \sum_{i=1}^N r'_i = -\frac{p_0}{\rho R_0^2} p'. \quad (10)$$

171 Using Eq. 6, the global resonance and damping factor can be readily found as a function of
 172 the complex averaged function K^* as

$$\omega_{res}^2 = \omega_0^2 \left(1 - \Re(K^*) \frac{\omega^2}{\omega_0^2} \right); \quad \zeta = -\Im(K^*); \quad K^* = \frac{\langle K_i^* r'_i \rangle}{\langle r'_i \rangle}. \quad (11)$$

173 where the symbol $\langle \cdot \rangle$ denotes the average over all the bubbles in the screen.

174 B. Synchronous solution for an infinite bubbly screen with crystal configuration

175 We start considering the synchronous solution for an infinite bubbly screen with equal
 176 amplitude for the radial motion of all bubbles. In this limit, $r'_i = r'_j = r'$, $\mathfrak{K}_i = \mathfrak{K}_j = \mathfrak{K}$,

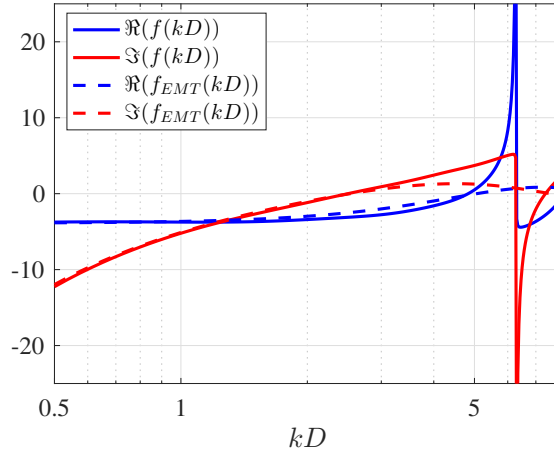


FIG. 2. Real and imaginary part of the function $f(kD)$. For reference we include the predictions of the effective medium theory. The solid line is corresponding to the $f(kD)$ and the dashed line is corresponding to EMT. The blue line is the real part, and the red line is the imaginary part. $N_l = 12000$ is used to keep $f(kD)$ converge.

177 $Q_i^* = 0$, and the solution of the system is thus given by the simplified expression

$$K_i^* = K^* = \mathfrak{K} - ikR_0(1 + \mathfrak{K})^2, \quad (12)$$

178 where $\mathfrak{K} = \frac{R_0}{D} f(kD)$ is a function that is proportional to the bubble inter-spacing parameter
 179 R_0/D and function

$$f(kD) = \sum_{j \neq i}^{\infty} \frac{e^{-ikD\tilde{d}_{ij}}}{\tilde{d}_{ij}} \quad (13)$$

180 depends on the dimensionless wavenumber kD and the particular geometry considered only.

181 Notice that, so far, the subscript i is still hold here to represent the bubble inside the infinite

182 bubbly screen under consideration, but that $f(kD)$ doesn't change with respect to the choice

183 of the bubble i . Taking advantage of rotation invariance of the system, the value of this

184 function can be obtained from a double sum over the layers surrounding an arbitrary bubble

$$f(kD) = \sum_{l=1}^{\infty} \frac{4}{l} e^{-ikDl} \left(1 + \sum_{q=1}^l \frac{2}{\sqrt{1+(q/l)^2}} e^{ikDl(1-\sqrt{1+(q/l)^2})} \right). \quad (14)$$

Eq. 14 can be evaluated numerically except in very particular cases. For instance, if $kD = 2\pi n$ with n being an integer, the first term will be a diverging harmonic series implying zero resonance frequency and infinite attenuation. We identify this phenomenon with a resonance phenomenon in the **spacing** within the bubbles. The convergence properties of this series in a general case are discussed in Appendix B. It is interesting to note that the results obtained are in agreement with the expression proposed by Leroy *et al.* (2009) who, taking advantage of an homogenization approach and introducing a cutoff length $b = D/\sqrt{\pi}$, obtain \mathfrak{K} using the bubble density $n_d = 1/D^2$ (number of bubbles per unit area in the screen) as

$$\mathfrak{K}_{\text{EMT}} = \frac{R_0}{D} f_{\text{EMT}}(kD) \approx \int_b^{\infty} \frac{R_0}{r} e^{-ikr} 2\pi r n_d dr = \frac{R_0}{D} f_{\text{EMT}}(kD), \quad (15)$$

$$f_{\text{EMT}}(kD) = -\frac{2\pi}{kD} (\sin(kb) + i \cos(kb)). \quad (16)$$

As shown by Pham *et al.* (2021), this expression is similar to the extension of the asymptotic analyses proposed by Cafisch *et al.* (1985) and later extended by Miksis and Ting (1989) to the second order, where the correction due to the collective effects of the bubbly screen is (Pham *et al.*, 2021)

$$f_{\text{EMT}}(kD) = -3.9 - i \frac{2\pi}{kD}. \quad (17)$$

Using the small angle approximation, it is straightforward to see that Eqs. 17 and 16 are equivalent and, as shown in Figure 2, reproduce well the values of the series for $kD \lesssim 3$ without the need of introducing any fitting parameter. In what follows we denote the predictions of this model as effective medium theory (EMT). Note that although the function

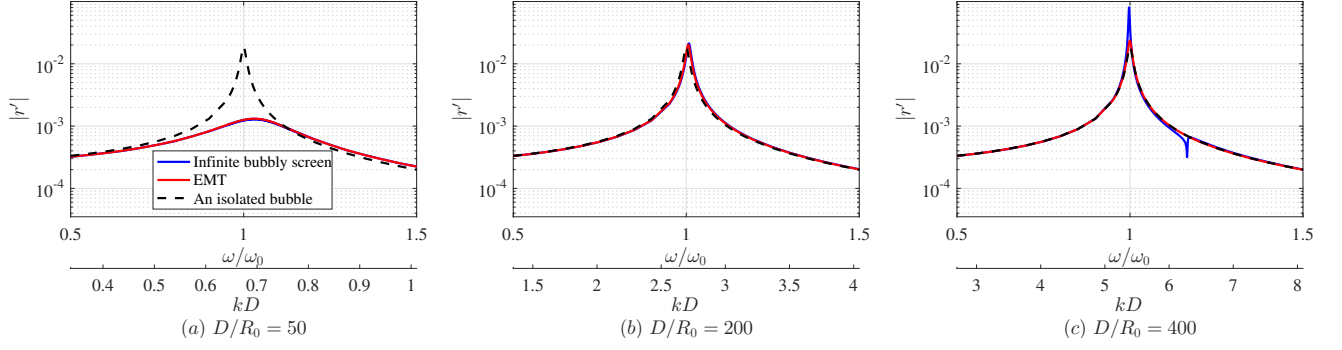


FIG. 3. Non-dimensional amplitude of the bubble oscillation in an infinite bubbly screen $|r'|$ as a function of ω/ω_0 for three different concentrations. The series are evaluated using $N_l = 12000$ layers. The curves predicted by EMT and the current model fit well with each other when $\frac{D}{R_0} = 50$ and gradually trend to the isolated bubble situation when $\frac{D}{R_0} = 200$. For $\frac{D}{R_0} = 400$, EMT recovers the solution of the single bubble case missing the resonance phenomenon captured by the current model.

202 $f(kD)$ is correctly predicted, EMT still neglect the correction of order $(kR_0 \cdot \Re)$ in the
 203 bubble dynamic motion.

204

205 Figure 3 represents the nondimensional amplitude of the bubble oscillation $|r'|$ as a func-
 206 tion of the frequency for three different concentrations for $\frac{p_0}{\rho R_0^2 \omega_0^2} = 0.25$ and $|p'| = 10^{-3} p_0$.
 207 For high concentrations ($D/R_0 = 50$) the resonance peak is damped, this effect being well
 208 captured by the EMT. As the bubble concentration is decreased, EMT recovers the solution
 209 of the single bubble case missing the resonance phenomenon captured by the current model.
 210 Remarkably, the intensity of the peak at resonance becomes much more important than the
 211 one predicted by the EMT with the increasing of kD . To gain further insight, Figure 4 shows

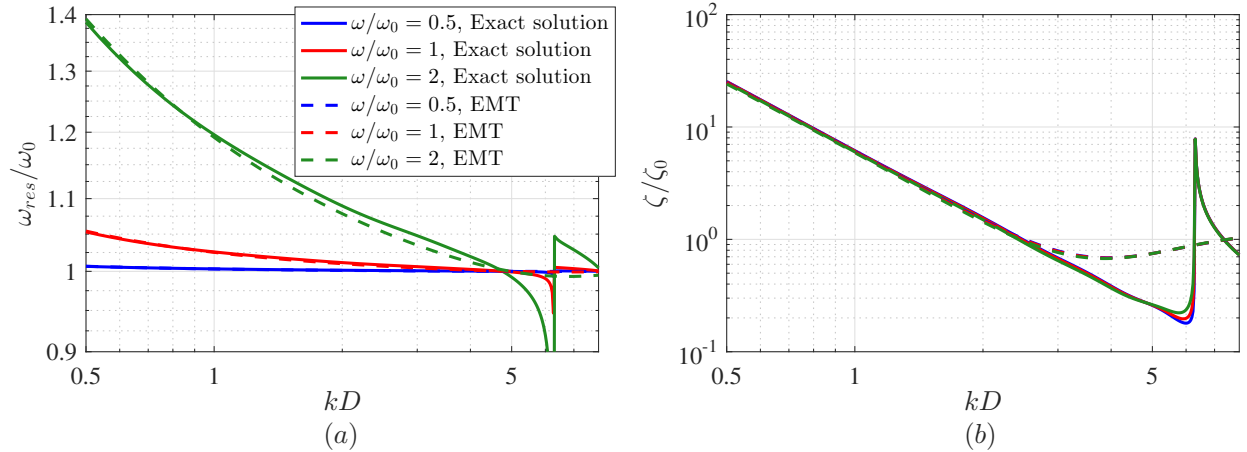


FIG. 4. (Left) Concentration effects on ω_{res}/ω_0 and (right) on ζ/ζ_0 . Solid lines are used for the approximated exact solution ($N_l = 12000$). Dashed lines represent the solution provided by the effective medium theory. The frequencies used are $\omega/\omega_0 = 0.5, 1, 2$ for blue, red and green line respectively.

212 the influence of D/R_0 at constant forcing frequency on the global resonance and the global
 213 damping factor. By changing the inter-bubble distance, the proposed model recovers well
 214 the predictions of the effective medium approximation for $kD \lesssim 3$, while for large values of
 215 kD both models give different predictions. This discrepancy is attributed to the difference
 216 between crystal structure and the random bubble distribution as discussed later on for a
 217 finite bubbly screen. In the effective medium approximation, bubbles are continuously and
 218 homogeneously distributed in the space, and the oscillating term $e^{-ikD\tilde{d}_{ij}}$ is thus smoothed
 219 out. The current model is able to capture the resonance effects originated for particular
 220 configurations. In the particular example shown here, it is expected to find a first resonance
 221 for $kD = 2\pi$, corresponding to the appearance of the resonance induced by the inter-bubble

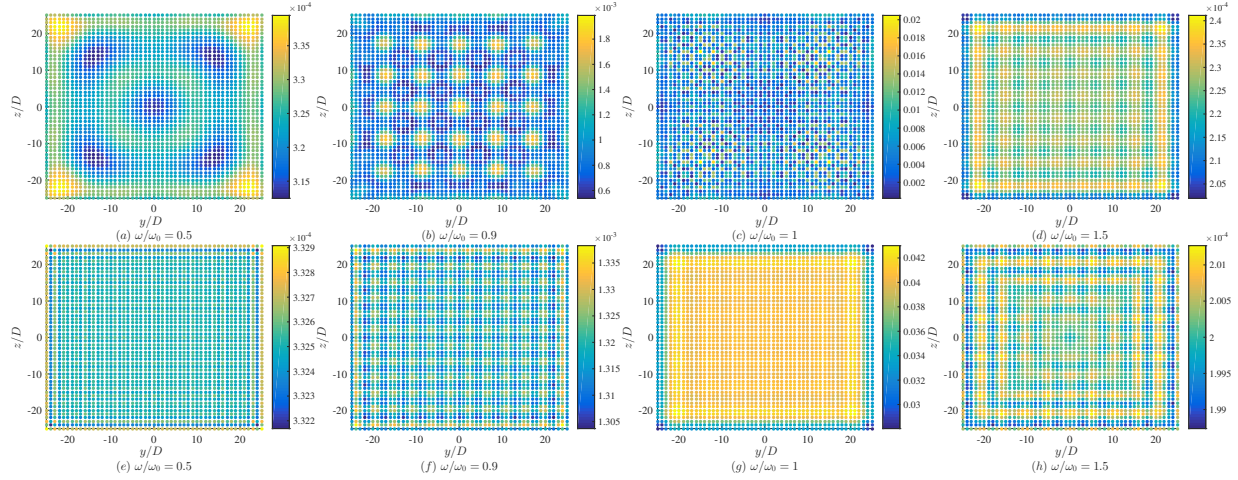


FIG. 5. Distribution of the amplitude of the nondimensional bubble oscillation $|r'_i|$ for different values of ω/ω_0 in a 51×51 bubbly screen for (top) $D/R_0 = 50$ ($kD = 0.67$) and (bottom) $D/R_0 = 400$ ($kD = 5.4$).

222 distance.

223

224 C. Finite size bubbly screens

225 In many applications, the size of the bubbly screens is limited to few tens or hundreds
 226 of bubbles, and the infinite screen limit may not be applicable. Figure 5 shows examples
 227 of the distribution of the nondimensional bubble oscillation amplitude $|r'_i|$ for a 51×51
 228 bubbly screen excited at the single bubble resonance frequency for two different values of the
 229 dimensionless wavenumber: $kD = 0.67 < 1$ and $kD = 5.4$. Characteristic spatial patterns
 230 are easily identified at resonance conditions but also become visible for other specific values
 231 of the forcing frequency. This phenomenon is related to the appearance of multiple resonance

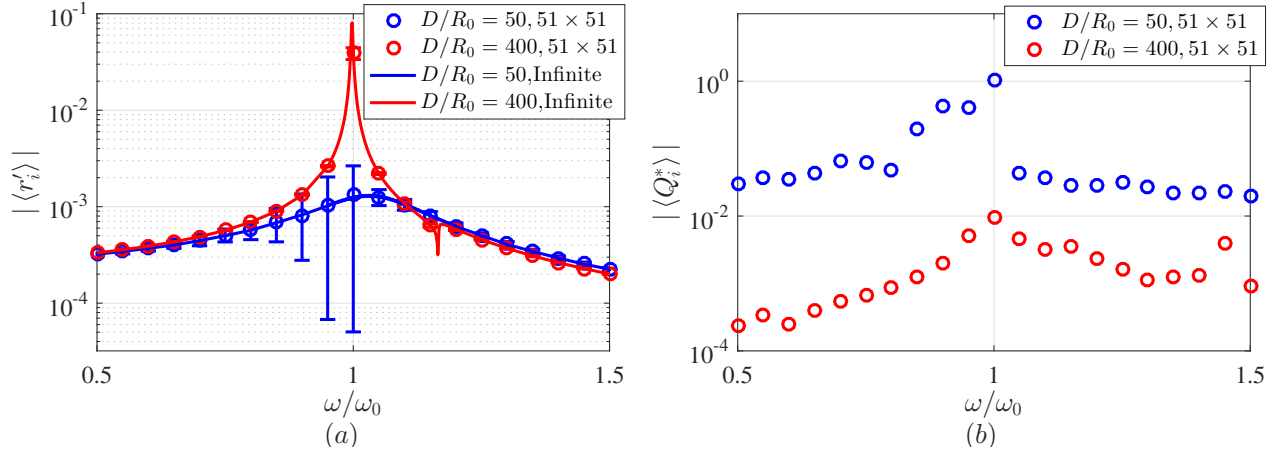


FIG. 6. (a) Averaged amplitude of the bubble oscillation $|\langle r'_i \rangle|$ (errorbar represents the standard deviation of $|\langle r'_i \rangle|$) and (b) $|\langle Q_i^* \rangle|$ of a 51×51 bubbly screen as a function of frequency.

233 frequencies in the system. Figure 6a shows that, as in the infinite case, the intensity of the
 234 mean value of r'_i becomes maximum at resonance, fitting the infinite bubbly screen well. The
 235 distribution of local resonance frequencies is represented using the intensity of the standard
 236 deviation of r'_i (errorbars in Figure 6a) and the averaged value of Q_i^* (Figure 6b) which tends
 237 to a plateau at larger frequencies and quickly decays for low frequencies.

238 The role of the concentration on $|\langle Q_i^* \rangle|$ is shown in Figure 7. At resonance (Figure 7b),
 239 we observe a sharp transition between $kD \leq 2$, where the fluctuations of $|\langle Q_i^* \rangle|$ become of
 240 order unity, and $kD > 2$, where $|\langle Q_i^* \rangle|$ takes significantly smaller values. Remarkably, in
 241 the regime of $kD \leq 2$, we do not see any clear asymptotic convergence to $|\langle Q_i^* \rangle| \rightarrow 0$ as
 242 we increase the number of bubbles in the screen. Below resonance (Figure 7a), the value of
 243 $|\langle Q_i^* \rangle|$ is small and slow convergence to zero is observed for the screens considered. One of
 244 the reasons for the slow convergence may be the excitation of non-uniform modes induced
 245 by boundary effects. The consequences of perturbation on the plane containing the bubbles

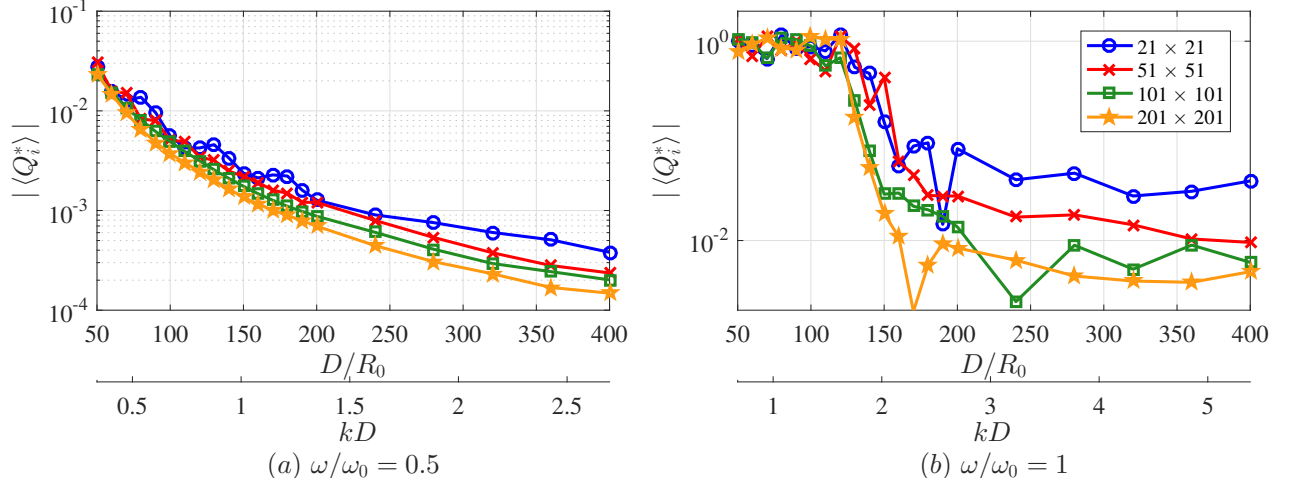


FIG. 7. Influence of concentration on $|\langle Q_i^* \rangle|$ for various finite size bubbly screens and two different values of ω/ω_0 .

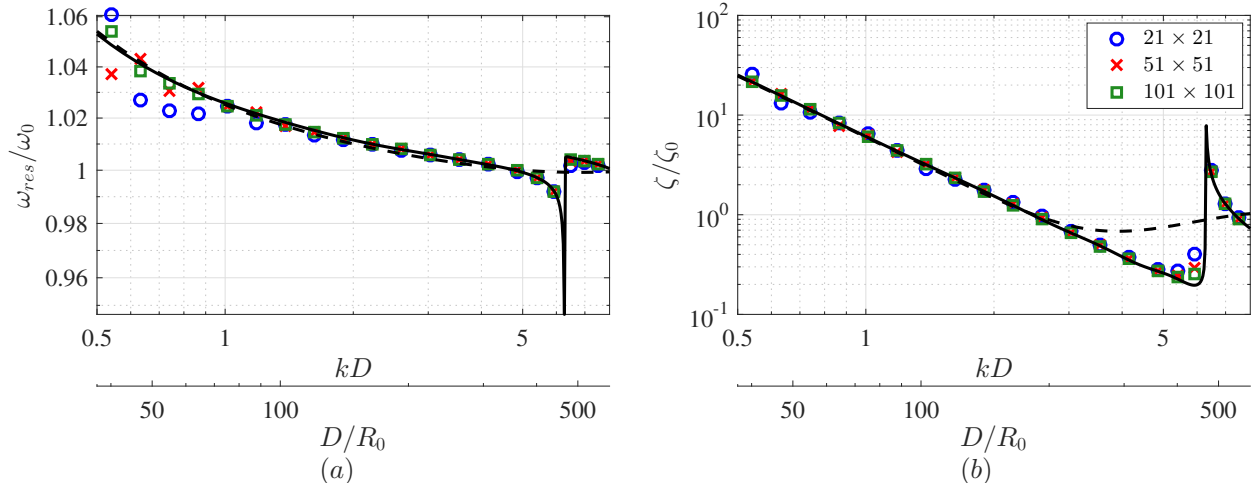


FIG. 8. Global resonance frequency and the global acoustical damping factor of finite bubbly screen with different screen sizes for $\omega/\omega_0 = 1$. 21×21 (blue circle), 51×51 (red cross sign) and 101×101 (green square). The theoretical curves calculated for an infinite system ($N_l = 12000$) and effective medium theory are included for reference (dashed line).

246 in the infinite case (we have imposed an unperturbed planar wave in the y-z plane) is left
247 for future works.

248

249 The effect of finite size effects on the global resonance frequency and the global damping
250 factor can be seen in Figure 8 for $\omega/\omega_0 = 1$. The infinite bubbly screen limit captures
251 accurately the averaged bubble response of the screen, only showing some small disagreement
252 for very concentrated systems, where we have seen the non-uniformity on the bubble response
253 is important.

254 D. Randomization

255 We further discuss the influence of the randomness on the position and on the polydisper-
256 sity of the bubbles separately. To that end, we firstly perturb the position of each bubble
257 by a random number $-\Theta_P < \theta_{y/z} < \Theta_P$ with respect to the crystal configuration so that i th
258 bubble is located at $\vec{x}_i = (0, y_i^{(c)} + \theta_{y,i}D, z_i^{(c)} + \theta_{z,i}D)$, where the superscript (c) stands for
259 variables corresponding to the crystal configuration. Figure 9(a,b) shows the global factors
260 defined in Eq. 11 averaged over 100 realizations for $\omega/\omega_0 = 1$ using a finite screen with
261 51×51 bubbles with different Θ_P . As expected, the resonance effects observed at $kD = 2\pi$
262 quickly vanish as the randomization parameter increases. Remarkably, the results obtained
263 differ from the effective medium theory for large values of the randomization parameter
264 and intermediate values of kD , the effect of randomization being especially visible on the
265 effective damping coefficient.

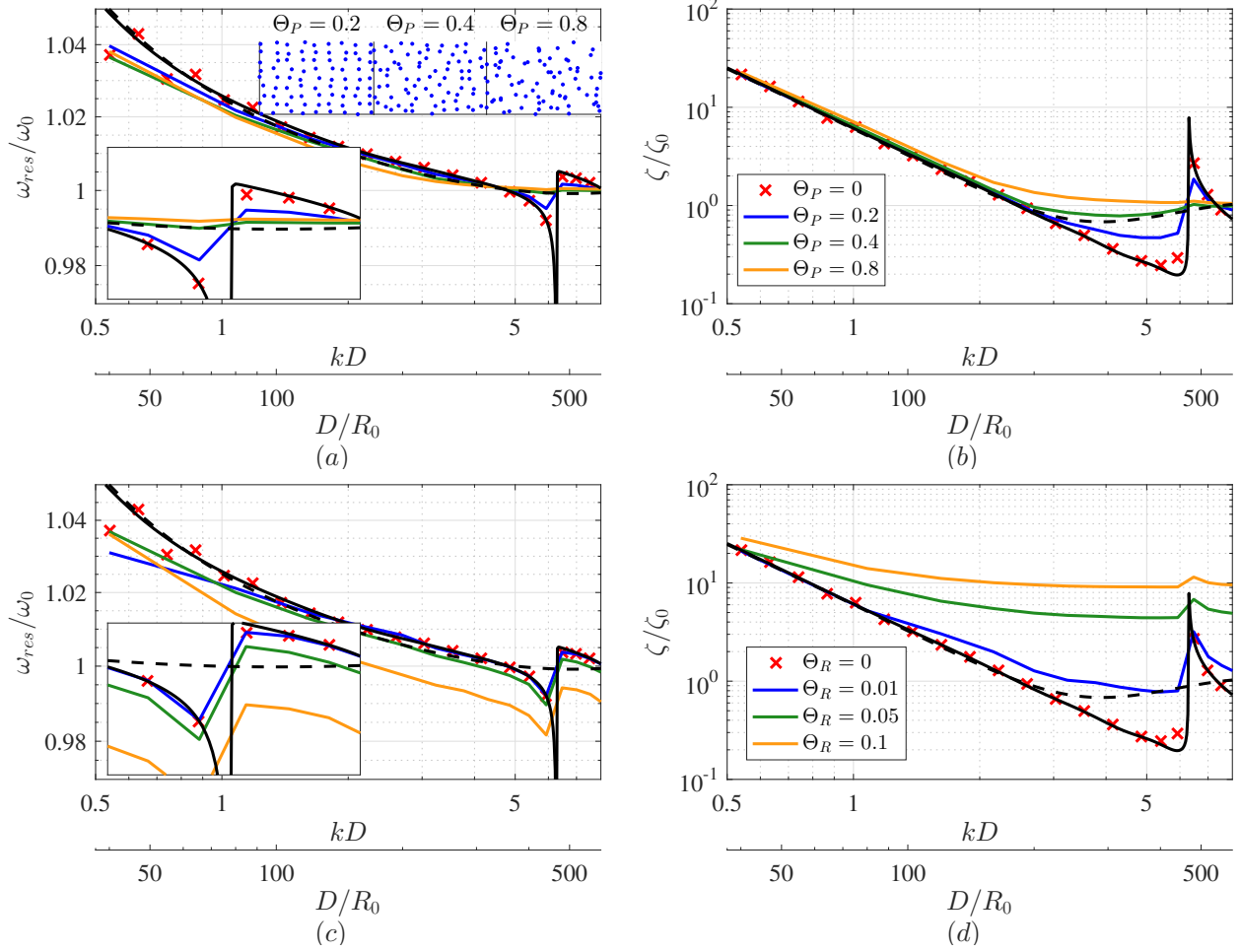


FIG. 9. Influence of (top) spatial randomness and (bottom) polydispersity for (left) the global resonance and (right) the global damping coefficient for a 51×51 finite bubbly screen using $\omega/\omega_0 = 1$. An example of the spatial distribution of the bubble positions is given in the inset of (a). For reference we include curves calculated for an infinite system (black solid line, $N_l = 12000$) and effective medium theory (dashed line).

266 In this case, both matrix $\mathbf{A}^{(0)}$ and $\mathbf{A}^{(1)}$ can be further decomposed as a globally uniform
 267 value given by the crystal structure and a correction directly attributed to randomization
 268 (see Appendix A). While the expectation of $\mathbf{A}^{(0)}$ is zero, the non-linear term in the $\mathbf{A}^{(1)}$
 269 matrix with respect to the position perturbation amplitude makes the averaged response

270 of the system to be different from the crystal situation for small perturbations. For large
 271 perturbations, the expectation of both $\mathbf{A}'^{(0)}$ and $\mathbf{A}'^{(1)}$ are a-priori different from zero and
 272 depend on the value of Θ_P . In such a situation, the difference between the fluctuation
 273 around the crystal configuration and the completely random distribution also makes the
 274 averaged response of the system to be different from EMT. In Figures 9(a,b) we see that the
 275 randomization intensity parameter Θ_P mainly increases the effective damping for $kD > 1$.

276 The influence of polydispersity is depicted in Figure 9(c,d). The equilibrium bubble
 277 radius of each bubble is perturbed with a random number $-\Theta_R < \theta_R < \Theta_R$ with respect
 278 to R_0 , such that $R_{i,0} = (1 + \theta_{R,i})R_0$. The same averaging process is repeated to obtain the
 279 global factors. As it occurs in the problem of linear wave propagation in bubbly liquids, the
 280 influence of polydispersity is mainly visible in the damping coefficients, playing a minor role
 281 on the shift of the resonance frequency. Notice that, different from the spatial randomness
 282 which is unavoidable restricted by the current technology, the polydisperse randomness plays
 283 a minor role in the experimental environments (Leroy *et al.*, 2009), and a detailed theoretical
 284 analysis is left for future publications.

285 IV. COMPRESSIBILITY EFFECTS IN THE NON-LINEAR REGIME

286 A. Numerical methods for differential equations with time delays

287 In the non-linear regime, it is no longer possible to find analytical solutions and one needs
 288 to solve the set of ODEs numerically. The differential equations considered can be written

$$\dot{y}(t) = f(t, y(t), y(t - \tau_1), \dots, y(t - \tau_n), \dot{y}(t - \tau_1), \dots, \dot{y}(t - \tau_n)), \quad (18)$$

where y is called state variable representing bubble radius or bubble wall velocity in our case. Traditionally, Eq. 18 is usually solved as ordinary differential equations, and the time-delay effect thus has to be ignored ($\tau_1, \dots, \tau_n = 0$). In this work, when non-linear effects become important, Eq. 18 is directly solved, treated as neutral delay differential equation (NDDE), which will reduce to general delay differential equation (DDE) if $\dot{y}(t) = f(t, y(t), y(t - \tau_1), \dots, y(t - \tau_n))$ and extend to state dependent NDDE if any of (τ_1, \dots, τ_n) is a function of state variable (Bellen and Zennaro, 2013). Integration of DDEs cannot be based on the mere adaption of some standard ODE code to the presence of delayed terms, which may dramatically modify the accuracy and stability of the underlying ODE method. To deal with NDDE, we first rewrite the Eq. 18 as:

$$\dot{y}(t) = f(y(t), y(t - \tau_1), \dots, y(t - \tau_n), \frac{y(t - \tau_1) - y(t - \tau_1 - \delta_t)}{\delta_t}, \dots, \frac{y(t - \tau_n) - y(t - \tau_n - \delta_t)}{\delta_t}) \quad (19)$$

which is the dissipative approximation of the NDDE and named as retarded DDE. For small enough δ_t , the retarded DDE solver will be stable as long as the neutral DDE is stable. Based on Eq. 19, implicit Runge–Kutta formulas taking advantage of continuous extensions is used, and the retarded DDE is solved accordingly with residual control. The works of Shampine (2005, 2008) are recommended for detailed mathematical principles.

For simulations in temporal domain, delays needed to be considered should always be finite. Notice that, for any simulations with finite duration, e.g., $[0, T]$, we only need to con-

308 sider the interactions from the bubbles with a distance from the bubble under consideration
309 less than $d_{ij} \leq cT$.

310 B. Numerical results

311 1. *Weakly non-linear regime*

312 One important aspect on the dynamic response of bubbly liquids is the appearance of
313 subharmonics, which ultimately indicates the first transition route to the chaotic response
314 obtained for large enough amplitude of excitation (Lauterborn and Cramer, 1981; Lauter-
315 born and Koch, 1987). The harmonic components of the acoustic wave scattered by bubbles
316 or ultrasound contrast agents are also important in medical applications (Halldorsdottir
317 *et al.*, 2011; Nio *et al.*, 2019). The harmonics emitted by bubbles has been described by
318 many authors (see Lauterborn and Kurz (2010) for a review), including studies for contrast
319 agents in a free field (Andersen and Jensen, 2009; Katiyar and Sarkar, 2011). More recently
320 Fan *et al.* (2020a) has revealed the impact of compressibility and bubble-wall interaction
321 effects on the subharmonic emission of a bubble in a rigid tube. However, the influence of
322 collective effects on the subharmonic emission has not been investigated in detail yet.

323

324 In this section, we compare the results obtained from the model presented for infinite
325 bubbly screens imposing synchronous motion ($R_i = R_j = R$) with the results obtained from
326 the EMT in non-linear regimes (Pham *et al.*, 2021) where

$$I_{EMT} = -2\pi c\dot{R}\frac{R^2}{D^2} + 3.9\frac{R}{D}(2\dot{R}^2 + \ddot{R}R). \quad (20)$$

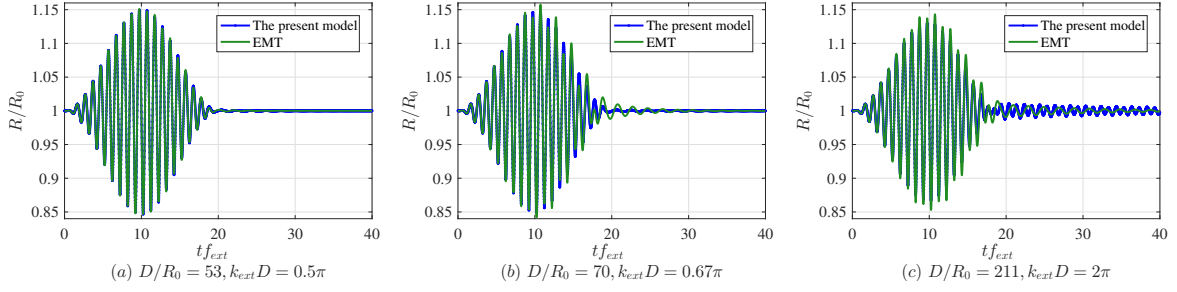


FIG. 10. Influence of concentration on the radius v.s. time curves. $p_a = 2p_0 = 2\text{bar}$, $f_{ext} = 2f_0 = 1.409\text{MHz}$, and $R_0 = 5\mu\text{m}$.

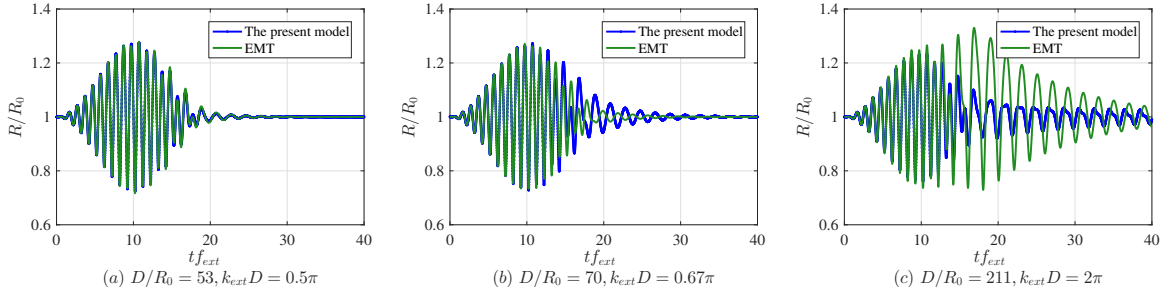


FIG. 11. Influence of concentration on the radius v.s. time curves. $p_a = 3.5p_0 = 3.5\text{bar}$, $f_{ext} = 2f_0 = 1.409\text{MHz}$, and $R_0 = 5\mu\text{m}$.

327 To that end, we excite the bubbly screen with an incident pulse of the form

$$p_\infty(t) = p_0 - p_a \frac{1}{2} \left[1 - \cos\left(\frac{\omega_{ext}}{N_c} t\right) \right] \sin(\omega_{ext} t), \quad (21)$$

328 where $N_c = 20$, and $\omega_{ext} = 2\omega_0$ in order to favor the appearance of a stable subharmonic
 329 response. For simplicity, in this subsection we will only consider the response of an infinite
 330 bubble screen.

331

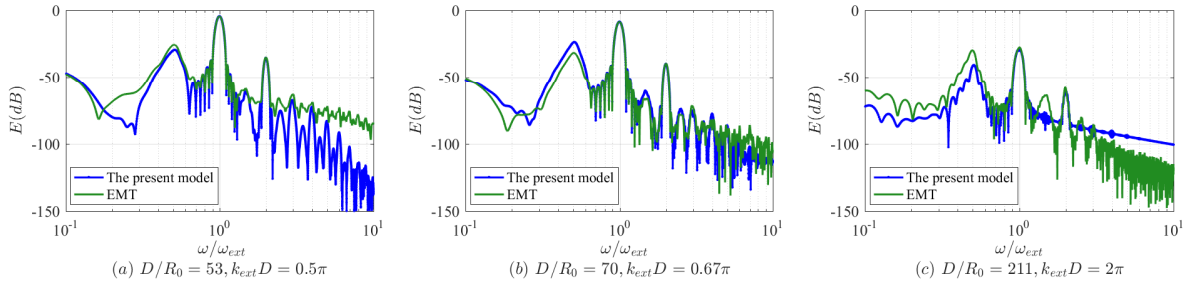


FIG. 12. The frequency spectrum of the present model and EMT using $p_a/p_0 = 3.5$. The energy is calculated by $E = 20 \log_{10} \left(\frac{|\mathfrak{F}(p_{rad})|}{|\mathfrak{F}(p_{rad})_{max}|} \right)$, where $|\mathfrak{F}(p_{rad})_{max}|$ is highest energy observed among all simulations.

332 In Figures 10-11, we can see the influence of concentration on the dynamic response of
 333 an infinite bubbly screen for two different excitation amplitudes. Consistent with the results
 334 in the linear regime, the effective medium model converges to the present model when the
 335 value of D/R_0 , and therefore, $k_{ext}D$ is small. The differences between two models become
 336 significant with the increase of p_a/p_0 and $k_{ext}D$. Even in the case, where the differences
 337 between the two models are important (Figure 11c), both models fit relatively well for small
 338 times, and gradually become different only after some time. One explanation could be that
 339 in-phase and out-phase interactions coming from different layers at different time cancel
 340 each other and increase oscillatingly. Besides, the fact that the differences between models
 341 become visible after some time seem to indicate the differences of the EMT and the current
 342 model on the bifurcation diagrams (Lauterborn and Kurz, 2010).

343

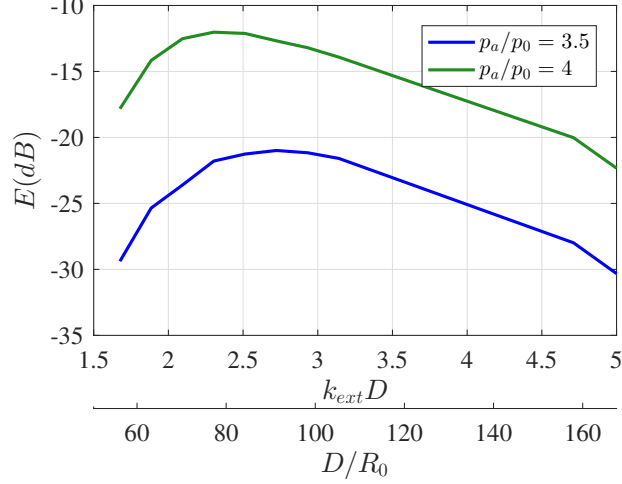


FIG. 13. Energy of the subharmonic emission as a function of concentration for a constant excitation frequency in a crystal structure.

344 Figure 12 shows the energy in the frequency spectrum of the infinite bubbly screen as a
 345 function of the bubble concentration from the radiated pressure (Pham *et al.*, 2021):

$$p_{rad} = 2\pi\rho c \frac{R^2 \dot{R}}{D^2}. \quad (22)$$

346 The energy is calculated as $E = 20\log_{10}\left(\frac{|\mathfrak{F}(p_{rad})|}{|\mathfrak{F}(p_{rad})_{max}|}\right)$, where $\mathfrak{F}(\cdot)$ is the Fourier transform,
 347 and $|\mathfrak{F}(p_{rad})_{max}|$ is highest energy observed among all simulations. Because the frequency
 348 of the subharmonics slightly shifts from $\frac{\omega_{ext}}{2}$ with the increasing of the amplitude of the
 349 driving pressure wave, the corresponding energy is chosen according to the peak amplitude
 350 rather than energy at $\frac{\omega_{ext}}{2}$. As expected the energy on the fundamental component increases
 351 as D/R_0 decreases due to the increase of bubble concentration (Figure 12). The overall
 352 spectrum is well reproduced by the EMT except for $kD = 2\pi$, where we clearly see how the
 353 spectrum predicted by the EMT contains a significantly higher level of energy mainly con-
 354 centrated at the subharmonics. In Figure 13, we show that optimal subharmonic emission

355 conditions appears for $k_{ext}D = [0.65, 0.75]\pi$ as a consequence of the crystal configuration.

356 This effect is not captured by the EMT.

357

358 **2. Strongly non-linear regime**

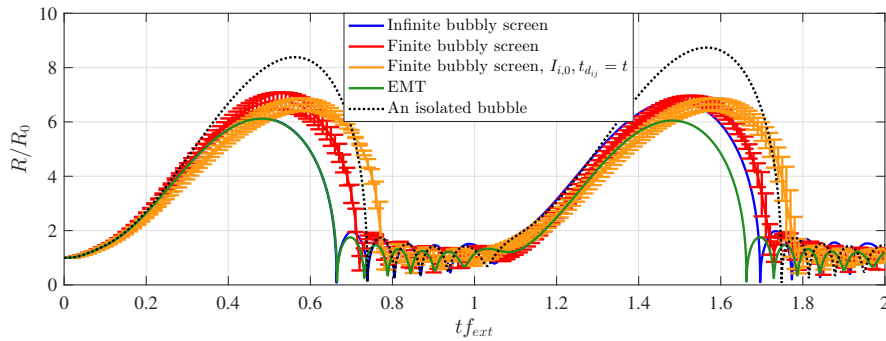


FIG. 14. Radius versus time curves predicted by different models for $D/R_0 = 134$ for an infinite bubbly screen oscillating synchronously and a 11×11 bubbly screen. $p_a = 2p_0 = 2bar$, $f_{ext} = 0.1f_0 = 70.461kHz$, and $R_0 = 5\mu m$. EMT and the infinite bubbly screen fit each other well up to the first rebound. In the later case, we show the averaged and the standard deviation of the bubble radius using the full model (red line) and the incompressible model with $I_i = I_{i,0}$ and $t_{d_{ij}} = t$ (yellow line).

When the excitation frequency is decreased ($\omega_{ext}/\omega_0 = 0.1$), the response of the bubbles become highly non-linear with a clear distinction between the expansion phase and the collapse and rebound region. In order to reduce the simulation time and transient effects, in this section we excite a bubbly screen with a perfect crystal configuration with an incident

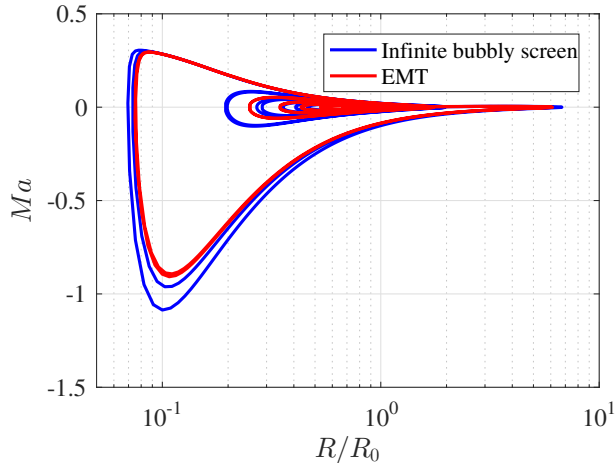


FIG. 15. Comparison of the trajectory of the averaged bubble radius versus $Ma = \dot{R}/c$ for the current model and the EMT.

planar wave represented by

$$p_{\infty}(t) = p_0 - p_a \sin(\omega_{ext}t).$$

359 The predictions of the temporal evolution of the bubble radius predicted by different models
 360 are given in Figure 14 for both infinite bubbly screens and finite bubbly screens. The am-
 361 plitude of the initial expansion in all cases is decreased compared to the isolating oscillating
 362 bubble. The results from the EMT fit well the results of the infinite bubbly screen in the
 363 first expansion. The difference of the radial dynamics between different models appear in
 364 the rebound stage (Figure 15), when the Mach number (\dot{R}/c) becomes important, so does
 365 the first order compressibility correction terms.

366

367 For completeness, in Figure 14 we also include the full simulation of a 11×11 bubbly
 368 screens. Because in this case bubble motion is no longer assumed to be synchronous, we

369 represent the averaged bubble radius among all bubbles in the screen as well as the standard
370 deviation in one realization. The influence of the interactions on the finite screen is reduced
371 in the expansion and is less strong comparing to the infinite case. Compressible effects play a
372 visible role despite the long wavelength of the incident wave, and the classical incompressible
373 bubble interaction model tends to over-predict the collapse time.

374 V. CONCLUSION

375 In this work, the compressibility effect on the bubble-bubble interaction is discussed. The
376 model proposed in [Fuster and Colonius \(2011\)](#) is particularized to explicitly write a system
377 of equations that account for first order correction compressibility effects. These effects are
378 shown to be important compared with the classical incompressible interaction mechanism
379 in Rayleigh–Plesset models.

380

381 In the linear regime, time-delay effects are always critical to capture the overall system
382 response of large bubble screens. We show that the current model recovers the effective
383 medium theory results up to second order for infinite crystal structures at large wavelengths
384 ($kD \lesssim 3$). In addition, the model is able to capture resonant conditions in diluted systems
385 due to crystal configurations that are not captured by averaged models. Randomization
386 on the bubble position and boundary effects on **bubbly screens of finite size** are shown to
387 be responsible to the appearance of characteristic periodic structures in the screen. These
388 effects can modify the global damping measured under some conditions.

389

390 In the non-linear oscillating regime, we numerically solve the proposed model as a neutral
 391 delay differential set of equations (NDDE). The fully incompressible model seems to be only
 392 suitable to predict the expansion phase and loses its accuracy during the strong collapse
 393 where compressibility effects play a major role and need to be included. Boundary size
 394 effects are shown to limit the applicability of the effective medium theory valid only for
 395 infinite systems.

396 ACKNOWLEDGMENTS

397 This research has been supported by NSFC, Project No. U1809212, No. U1709203 and
 398 No. 41576102.

399 APPENDIX A:

When $p'_i \ll 1$, the system of Eq. 4 can be written in matrix form $\mathbf{A}\vec{r}' = -\frac{p_0}{\rho R_0^2 \omega_0^2} \vec{p}'$ with
 $\mathbf{A} = (\mathbf{A}^{(0)} + ikR_0\mathbf{A}^{(1)})$, where

$$A_{ij}^{(0)} = \begin{cases} 1 - \left(\frac{\omega}{\omega_0}\right)^2 & \text{if } i = j, \\ -\left(\frac{\omega}{\omega_0}\right)^2 S_{ij} & i \neq j \end{cases}, A_{ij}^{(1)} = \begin{cases} \left(\frac{\omega}{\omega_0}\right)^2 (1 + \mathfrak{K}_i) - \mathfrak{K}_i & \text{if } i = j, \\ \left(\left(\frac{\omega}{\omega_0}\right)^2 (1 + \mathfrak{K}_i) + 1\right) S_{ij} & i \neq j \end{cases},$$

400 with $S_{ij} = \frac{R_0}{D} \frac{e^{-ikD\tilde{d}_{ij}}}{\tilde{d}_{ij}}$ and $\mathfrak{K}_i = \sum_{j \neq i}^N S_{ij}$.

In general cases using finite bubbly screen, bubbles may be not spatially arranged perfectly, and it is possible to rewrite this system by separating variables S_{ij} and \mathfrak{K}_i into a crystal contribution and a spatially fluctuating part attributed to the perturbation of bub-

bles position

$$S_{ij} = S_{ij}^{(c)} + S'_{ij},$$

$$\mathfrak{K}_i = \mathfrak{K}_i^{(c)} + \mathfrak{K}'_i = \sum_{j \neq i}^N S_{ij}^{(c)} + \sum_{j \neq i}^N S'_{ij},$$

401 where the superscript ^(c) stands for variables corresponding to the crystal configuration, and
 402 the distances between bubbles is written as $\tilde{d}_{ij} = \tilde{d}_{ij}^{(c)} + \tilde{d}'_{ij}$. In this case, matrix \mathbf{A} can be
 403 further decomposed as $\mathbf{A} \approx \mathbf{A}^{(C)} + \mathbf{A}'$ where $\mathbf{A}^{(C)}$ represents the value of \mathbf{A} obtained with
 404 the values of a crystal structure and \mathbf{A}' is the fluctuating part

$$A'_{ij}{}^{(0)} = \begin{cases} 0 & \text{if } i = j, \\ -\left(\frac{\omega}{\omega_0}\right)^2 S'_{ij} & \text{otherwise,} \end{cases}$$

$$A'_{ij}{}^{(1)} = \begin{cases} \left(\left(\frac{\omega}{\omega_0}\right)^2 - 1\right) \mathfrak{K}'_i & \text{if } i = j, \\ \left(\left(\frac{\omega}{\omega_0}\right)^2 + 1\right) S'_{ij} + \left(\frac{\omega}{\omega_0}\right)^2 (\mathfrak{K}'_i S'_{ij} + \mathfrak{K}_i^{(c)} S'_{ij} + \mathfrak{K}'_i S_{ij}^{(c)}) & \text{otherwise.} \end{cases}$$

When the position perturbation is small, taking advantage of Taylor expansion, we have:

$$S'_{ij} \approx -ikD\tilde{d}'_{ij} \frac{R_0 e^{-ikD\tilde{d}_{ij}^{(c)}}}{D \tilde{d}_{ij}^{(c)}}.$$

405 In such a situation, the expectation of $A'_{ij}{}^{(0)}$ is zero as long as the expectation of \tilde{d}'_{ij} is zero.
 406 However the expectation of the $\mathfrak{K}'_i S'_{ij}$ term appearing in $A'_{ij}{}^{(1)}$, which acts like a variance
 407 term, is different from zero even for the small perturbations. Obviously when the amplitude
 408 of perturbation \tilde{d}'_{ij} is large, the expectation of both $A'_{ij}{}^{(0)}$ and $A'_{ij}{}^{(1)}$ are a-priori different from
 409 zero.

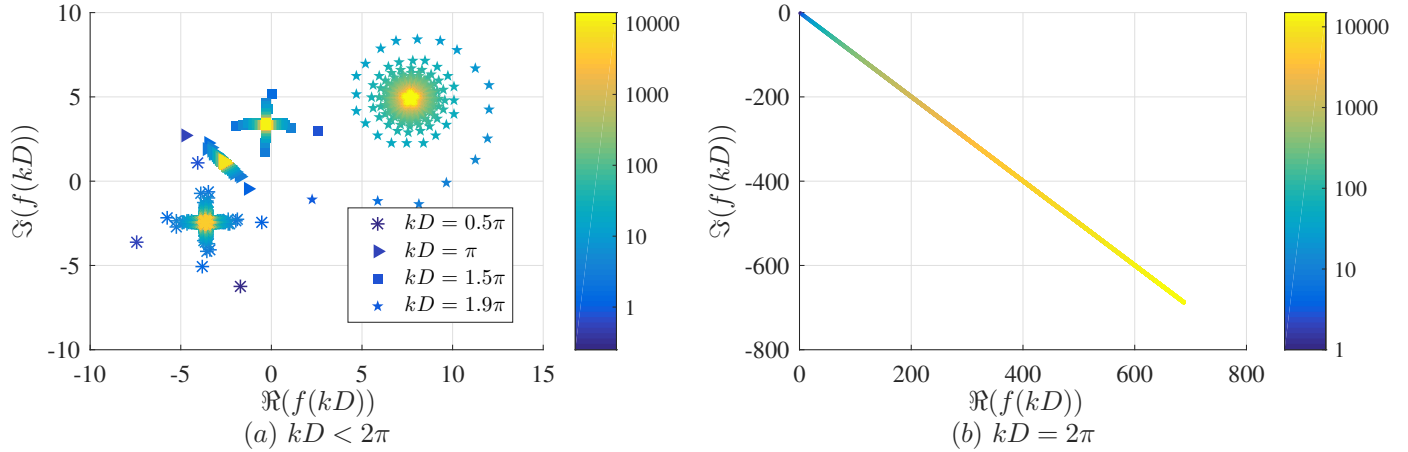


FIG. 16. Influence of the truncation N_l on the evaluation of the series in Eq. 14 for a crystal infinite screen and different values of kD . The colorbar represents the nondimensional truncation distance $N_l \frac{D}{\lambda}$.

410 APPENDIX B:

411 The convergence of the infinite series

$$f(kD) = \sum_{l=1}^{\infty} \frac{4}{l} e^{-ikDl} \left(1 + \sum_{q=1}^l \frac{2}{\sqrt{1 + (q/l)^2}} e^{ikDl(1 - \sqrt{1 + (q/l)^2})} \right)$$

412 is discussed as follows. For sufficiently large value of l , because quantity $p = \sqrt{1 + (q/l)^2}$ is

413 bounded between 1 and $\sqrt{2}$, we can approximate the series as

$$\sum_{q=1}^l \frac{2}{\sqrt{1 + (q/l)^2}} e^{ikDl(1 - \sqrt{1 + (q/l)^2})} \approx \int_1^{\sqrt{2}} \frac{2}{p} e^{ikDl(1-p)} dp = 2e^{ikDl} \left(E_{1/2}(ikDl) - 2^{1/4} E_{1/2}(\sqrt{2}ikDl) \right),$$

where $E(x)$ is the exponential integral function. Taking the limit for $l \rightarrow \infty$, we readily find that

$$\lim_{l \rightarrow \infty} \left(E_{1/2}(ikDl) - 2^{1/4} E_{1/2}(\sqrt{2}ikDl) \right) = 0$$

implying that this term always converges. The convergence of the series is then discussed in terms of the convergence of

$$\sum_{l=1}^{\infty} \frac{4}{l} e^{-ikDl} = \sum_{l=1}^{\infty} 4 \frac{z^l}{l} = 4 \ln \left(\frac{1}{1-z} \right)$$

414 where $z = e^{-ikD}$. For $kD = 2\pi n$ the series diverges and it converges otherwise. The influ-
415 ence of the number of layers considered on the series is reported in Figure 16 for different
416 values of kD . In general, a very large value of the number of layers is required to accurately
417 represent the infinity limit.

418

419

420 Andersen, K. S., and Jensen, J. A. (2009). “Ambient pressure sensitivity of microbubbles
421 investigated through a parameter study,” *The Journal of the Acoustical Society of America*
422 **126**(6), 3350–3358.

423 Bellen, A., and Zennaro, M. (2013). *Numerical methods for delay differential equations*
424 (Oxford university press).

425 Bergamasco, L., and Fuster, D. (2017). “Oscillation regimes of gas/vapor bubbles,” *Inter-*
426 *national Journal of Heat and Mass Transfer* **112**(), 72–80.

427 Bremond, N., Arora, M., Ohl, C.-D., and Lohse, D. (2006). “Controlled multibubble surface
428 cavitation,” *Physical review letters* **96**(22), 224501.

429 Caffisch, R. E., Miksis, M. J., Papanicolaou, G. C., and Ting, L. (1985). “Effective equations
430 for wave propagation in bubbly liquids,” *Journal of Fluid Mechanics* **153**, 259–273.

431 Commander, K. W., and Prosperetti, A. (1989). “Linear pressure waves in bubbly liquids:
432 Comparison between theory and experiments,” *The Journal of the Acoustical Society of*
433 *America* **85**(2), 732–746.

434 Coussios, C. C., and Roy, R. A. (2008). “Applications of acoustics and cavitation to nonin-
435 vasive therapy and drug delivery,” *Annu. Rev. Fluid Mech.* **40**, 395–420.

436 Dahl, P. H., and Kapodistrias, G. (2003). “Scattering from a single bubble near a rough-
437 ened air–water interface: Laboratory measurements and modeling,” *The Journal of the*
438 *Acoustical Society of America* **113**(1), 94–101.

439 Devaud, M., Hocquet, T., and Leroy, V. (2010). “Sound propagation in a monodisperse
440 bubble cloud: From the crystal to the glass,” *The European Physical Journal E* **32**(1),
441 13–23.

442 Doinikov, A. A., Manasseh, R., and Ooi, A. (2005). “Time delays in coupled multibubble
443 systems (I),” *The Journal of the Acoustical Society of America* **117**(1), 47–50.

444 Faez, T., Emmer, M., Kooiman, K., Versluis, M., van der Steen, A. F., and de Jong, N.
445 (2012). “20 years of ultrasound contrast agent modeling,” *IEEE transactions on ultrason-*
446 *ics, ferroelectrics, and frequency control* **60**(1), 7–20.

447 Fan, Y., Li, H., and Fuster, D. (2020a). “Optimal subharmonic emission of stable bubble
448 oscillations in a tube,” *Physical Review E* **102**(1), 013105.

449 Fan, Y., Li, H., Zhu, J., and Du, W. (2020b). “A simple model of bubble cluster dynamics
450 in an acoustic field,” *Ultrasonics sonochemistry* **64**, 104790.

451 Foldy, L. L. (1945). “The multiple scattering of waves. i. general theory of isotropic scat-
452 tering by randomly distributed scatterers,” *Physical review* **67**(3-4), 107.

453 Fuster, D. (2019). “A review of models for bubble clusters in cavitating flows,” *Flow, Tur-*
454 *bulence and Combustion* **102**(3), 497–536.

455 Fuster, D., and Colonius, T. (2011). “Modelling bubble clusters in compressible liquids,”
456 *Journal of Fluid Mechanics* **688**, 352–389.

457 Fuster, D., and Montel, F. (2015). “Mass transfer effects on linear wave propagation in
458 diluted bubbly liquids,” *Journal of Fluid Mechanics* **779**, 598–621.

459 Gilmore, F. R. (1952). “The growth or collapse of a spherical bubble in a viscous compress-
460 ible liquid,” .

461 Halldorsdottir, V. G., Dave, J. K., Leodore, L. M., Eisenbrey, J. R., Park, S., Hall, A. L.,
462 Thomenius, K., and Forsberg, F. (2011). “Subharmonic contrast microbubble signals for
463 noninvasive pressure estimation under static and dynamic flow conditions,” *Ultrasonic*
464 *imaging* **33**(3), 153–164.

465 Ida, M., Naoe, T., and Futakawa, M. (2007). “Suppression of cavitation inception by gas
466 bubble injection: A numerical study focusing on bubble-bubble interaction,” *Physical*
467 *Review E* **76**(4), 046309.

468 Ilinskii, Y. A., Hamilton, M. F., and Zabolotskaya, E. A. (2007). “Bubble interaction dy-
469 namics in lagrangian and hamiltonian mechanics,” *The Journal of the Acoustical Society*
470 *of America* **121**(2), 786–795.

471 Katiyar, A., and Sarkar, K. (2011). “Excitation threshold for subharmonic generation from
472 contrast microbubbles,” *The Journal of the Acoustical Society of America* **130**(5), 3137–
473 3147.

474 Keller, J. B., and Miksis, M. (1980). “Bubble oscillations of large amplitude,” The Journal
475 of the Acoustical Society of America **68**(2), 628–633.

476 Lauterborn, W., and Cramer, E. (1981). “Subharmonic route to chaos observed in acous-
477 tics,” Physical Review Letters **47**(20), 1445.

478 Lauterborn, W., and Koch, A. (1987). “Holographic observation of period-doubled and
479 chaotic bubble oscillations in acoustic cavitation,” Physical Review A **35**(4), 1974.

480 Lauterborn, W., and Kurz, T. (2010). “Physics of bubble oscillations,” Reports on progress
481 in physics **73**(10), 106501.

482 Leroy, V., Strybulevych, A., Lanoy, M., Lemoult, F., Tourin, A., and Page, J. H. (2015).
483 “Superabsorption of acoustic waves with bubble metascreens,” Physical Review B **91**(2),
484 020301.

485 Leroy, V., Strybulevych, A., Scanlon, M., and Page, J. (2009). “Transmission of ultrasound
486 through a single layer of bubbles,” The European Physical Journal E **29**(1), 123–130.

487 Lohse, D. (2018). “Bubble puzzles: From fundamentals to applications,” Physical review
488 fluids **3**(11), 110504.

489 Lombard, O., Barrière, C., and Leroy, V. (2015). “Nonlinear multiple scattering of acoustic
490 waves by a layer of bubbles,” EPL (Europhysics Letters) **112**(2), 24002.

491 Maeda, K., and Colonius, T. (2019). “Bubble cloud dynamics in an ultrasound field,”
492 Journal of fluid mechanics **862**, 1105.

493 Manasseh, R., Nikolovska, A., Ooi, A., and Yoshida, S. (2004). “Anisotropy in the sound
494 field generated by a bubble chain,” Journal of Sound and Vibration **278**(4-5), 807–823.

495 Mettin, R., Akhatov, I., Parlitz, U., Ohl, C., and Lauterborn, W. (1997). “Bjerknes forces
496 between small cavitation bubbles in a strong acoustic field,” *Physical review E* **56**(3), 2924.

497 Miksis, M. J., and Ting, L. (1989). “Effects of bubbly layers on wave propagation,” *The*
498 *Journal of the Acoustical Society of America* **86**(6), 2349–2358.

499 Nio, A. Q., Faraci, A., Christensen-Jeffries, K., Raymond, J. L., Monaghan, M. J., Fuster,
500 D., Forsberg, F., Eckersley, R. J., and Lamata, P. (2019). “Optimal control of sonovue
501 microbubbles to estimate hydrostatic pressure,” *IEEE transactions on ultrasonics, ferro-*
502 *electrics, and frequency control* **67**(3), 557–567.

503 Okita, K., Sugiyama, K., Takagi, S., and Matsumoto, Y. (2013). “Microbubble behavior
504 in an ultrasound field for high intensity focused ultrasound therapy enhancement,” *The*
505 *Journal of the Acoustical Society of America* **134**(2), 1576–1585.

506 Ooi, A., Nikolovska, A., and Manasseh, R. (2008). “Analysis of time delay effects on a linear
507 bubble chain system,” *The Journal of the Acoustical Society of America* **124**(2), 815–826.

508 Pham, K., Mercier, J.-F., Fuster, D., Marigo, J.-J., and Maurel, A. (2021). “Scattering of
509 acoustic waves by a nonlinear resonant bubbly screen,” *Journal of Fluid Mechanics* **906**.

510 Prosperetti, A., Lezzi, A. *et al.* (1986). “Bubble dynamics in a compressible liquid. part 1.
511 first-order theory,” *J. FLUID MECH.*, 1986, **168**, 457–478.

512 Champine, L. (2005). “Solving odes and ddes with residual control,” *Applied Numerical*
513 *Mathematics* **52**(1), 113–127.

514 Champine, L. F. (2008). “Dissipative approximations to neutral ddes,” *Applied Mathematics*
515 *and Computation* **203**(2), 641–648.

516 Sujarittam, K., and Choi, J. J. (2020). “Angular dependence of the acoustic signal of a
517 microbubble cloud,” *The Journal of the Acoustical Society of America* **148**(5), 2958–2972.

518 van’t Wout, E., and Feuillade, C. (2021). “Proximity resonances of water-entrained air
519 bubbles near acoustically reflecting boundaries,” *The Journal of the Acoustical Society of*
520 *America* **149**(4), 2477–2491.

521 Yasui, K., Iida, Y., Tuziuti, T., Kozuka, T., and Towata, A. (2008). “Strongly interacting
522 bubbles under an ultrasonic horn,” *Physical Review E* **77**(1), 016609.

523 Ye, Z., and Feuillade, C. (1997). “Sound scattering by an air bubble near a plane sea
524 surface,” *The Journal of the Acoustical Society of America* **102**(2), 798–805.